J Solid State Electrochem (2004) 8: 626–632
DOI 10.1007/s10008-003-0485-6

ORIGINAL PAPER

Petra Fedtke · Marion Wienecke · Mihaela-C. Bunescu
Torsten Barfels · Klaus Deistung · Marlis Pietrzak

Yttria-stabilized zirconia films deposited by plasma spraying and sputtering

Received: 11 April 2003 / Accepted: 29 September 2003 / Published online: 21 February 2004

Abstract Thin films of yttria-stabilized zirconia (YSZ) deposited by sputtering and plasma spraying have been analysed as solid electrolyte for oxygen gas sensors and solid oxide fuel cells. Different substrates have been considered in order to provide good adhesion, dense electrolyte films, and mechanical and thermal stability. By optimization of the sputtering parameters, a Pt/YSZ/Pt assembly of 1.5 μm thickness and with an electrical resistance of 500 MΩ at room temperature has been obtained. The plasma-sprayed films (150 μm thickness) have shown oxygen ion conductivity with a reproducible sensitivity on oxygen partial pressure starting at 400 °C and an activation energy of ~1 eV. Lanthanum strontium manganate (350 μm thickness) was sprayed as cathode material.

Keywords Oxygen sensor · Plasma spraying · Solid oxide fuel cell · Sputtering · Yttria-stabilized zirconia

Introduction

Yttria-stabilized zirconia (YSZ) has been used for long time as solid electrolyte in various electrochemical devices, which require oxygen ion conductivity (oxygen gas sensors, solid oxide fuel cells, oxygen pumps, etc.). The most applied type was the bulk ceramic, but recently thin films have been also considered due to several advantages: reduced ohmic losses, lower operating temperatures, smaller dimensions, etc.

Presented at the OSSEP Workshop "Ionic and Mixed Conductors: Methods and Processes", Aveiro, Portugal, 10–12 April 2003

P. Fedtke (✉) · M. Wienecke · M.-C. Bunescu · T. Barfels
K. Deistung · M. Pietrzak
Institut für Oberflächen- und Dünnschichttechnik, Hochschule Wismar, Philipp-Müller-Strasse, 23952 Wismar, Germany
E-mail: p.fedtke@et.hs-wismar.de
Tel.: +49-3841-753413
Fax: +49-3841-753136

Chemical vapour deposition, evaporation, sol-gel, spray pyrolysis, d.c. and r.f. sputtering and plasma spraying are some of the processes reported for the deposition of YSZ thin films [1, 2, 3, 4, 5, 6, 7]. Reactive deposition sputtering has proved to be advantageous owing to lower working temperatures and a better stoichiometry of the film. Some of the disadvantages of this method are connected with pinholes, density of the films, and the adhesion to the substrate.

In this paper we report on YSZ thin films deposited by d.c. and r.f. sputtering and plasma spraying, applied as electrolyte for oxygen gas sensors and solid oxide fuel cells (SOFCs).

Experimental

Balzers PLS 500 equipment was used for d.c .and r.f. magnetron sputtering deposition of YSZ thin films at room temperature on various substrates. A metallic target with the composition Zr:Y (3N) = 84:16 at% was used. For the d.c. sputtering the parameters were: $P = 50$–80 W, Ar flow = 40–60 sccm, O_2 flow = 0–3 sccm, $p = 5.4$–7.4×10^{-3} mbar. For the r.f. sputtering the following deposition parameters were used: $P = 100$–200 W, Ar flow = 40–130 sccm, O_2 flow = 0–15 sccm, $p = 8.7$–15×10^{-3} mbar. Glass, silicon, sintered aluminium oxide and sapphire were used as substrates.

Thin films of platinum were deposited as electrodes for the electrochemical cell, one between the substrate and YSZ film and the second above the YSZ film, as shown in Fig. 1a. A specially shaped mask was used to create electrical contact paths. The sputtering parameters for the Pt films were: Ar flow = 48 sccm, $P = 50$ W, $p = 4.3\times10^{-3}$ mbar.

An atmospheric plasma spraying equipment, operating at $I = 600$ A, Ar flow = 45 l/min, H_2 flow = 14 l/min, spraying distance = 120 mm and gas flow for powder transport = 3 l/min, was used for the deposition of the SOFC element in one process, on steel and Ni-base alloy plates, as in Fig. 1b. Different mixtures of YSZ and 5–40% Ni powder were used for the anode material. A YSZ thin film was the electrolyte. The second electrode of the cell, the cathode, was a $La_{0.8}Sr_{0.2}MnO_3$ (LSM) ceramic deposited in the same process, above the YSZ electrolyte. Different precursor powders were tested:

1. For YSZ, the commercially available Sulzer Metco powder (1N), with an average grain dimension of 50 μm.

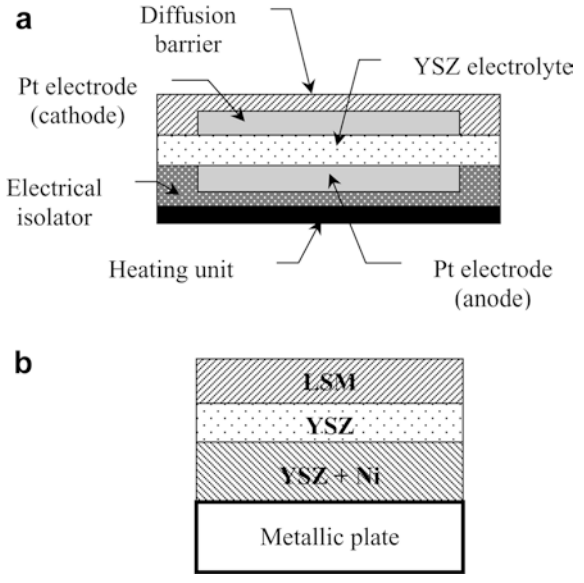

Fig. 1 Schematic presentation of (**a**) the sensor assembly and (**b**) the SOFC element

2. For the LSM cathode, both the commercially available EMPA powder (purity unknown), with grain dimension in the range 20–90 μm, and a mixture of appropriate amounts of La_2O_3 (3N), MnO_2 (3N) and $SrCO_3$ (3N), all from Aldrich.

Microstructure characterization of the deposited films was performed by SEM (Tesla BS 340), TEM (Philips CM 200), EDS (EDAX) and XRD (synchrotron radiation at Desy-Hasylab, beamline B2, $\lambda = 1.12$ Å). Impedance spectroscopy (type Zahner) was used to investigate the electrical resistivity of the films at different temperatures and oxygen partial pressures. The experimental parameters used were: $U = 20$ mV, $f = 100$ kHz to 50 mHz, $j_{O2} = 40$ vol ppm.

Results and discussion

Sputtering

The first steps in our experiments were assigned to the optimization of the deposition parameters. The flow rate of the working gases influences the stability of the process and the quality of the thin film. Thus, the graphs in Fig. 2 show the variation of the deposition rate versus argon and oxygen flow, measured for the r.f. sputtering. Variation of the argon flow in the interval 90–120 sccm at 150 W and 200 W deposition power did not produce significant changes in the deposition rate, which was about 300 nm/h for 200 W and 206 nm/h for 150 W.

The increase of the oxygen flow from 3 sccm to 6 sccm produced a sharp decrease of the deposition rate from 720 nm/h to 280 nm/h. For a further increase of oxygen flow up to 16 sccm the deposition rate was almost constant at 250 nm/h. The decrease of the deposition rate with an increase of the oxygen flow was explained by a lower sputter yield of oxygen compared to that of argon [3].

We have analysed the influence of the oxygen flow on the film thickness (determined by gravimetric measurement) deposited by d.c. sputtering for 20 min. An approximately constant value of 200 nm was measured for up to 1.4 sccm oxygen flow. For higher oxygen flows, up to 1.8 sccm, the film thickness strongly decreased to 75 nm (Fig. 3). The result can be explained by the oxidation of the target surface for the higher oxygen flow. For a further increase of the oxygen flow the plasma was unstable and the process was stopped. The TEM analyses have shown a small decrease of the grain dimension from 20 nm to 10 nm with increasing oxygen flow. Pinholes could be noticed in all samples, independent of the oxygen flow (Fig. 4). We consider that for thicker films this "defect" is healed by subsequent deposition of atoms, resulting in dense films.

The rings radius from the electron diffraction image fit relatively well to the cubic phase of $Y_{0.15}Zr_{0.85}O_{1.93}$ (YSZ), with $a = 5.13900$ Å, although the cubic and tetragonal phases have very similar interplanar distances that are difficult to resolve by electron diffraction.

Figure 5 shows the cross-section image of the Pt/YSZ/Pt assembly deposited on a flat glass substrate. Equiaxial grains rather than columnar, as small as 0.5 μm, can be observed, as well as a total thickness of the assembly of 1.5 μm. The platinum films (electrodes) are too thin to be resolved by this technique. For this film an electrical resistance of 500 MΩ at room temperature was measured. The oxygen ion conductivity measurements for the sputtered films are in progress.

By X-ray energy dispersive spectrometry (EDS) the local micro-composition of the thin YSZ films could be measured in the TEM. The results are presented in Fig. 6. Taking into account the errors of the method, we can appreciate a relatively constant and stoichiometric composition, independent of the oxygen flow.

The structure of the YSZ films r.f. sputtered on Al_2O_3 (4 h, 200 W, 80 sccm Ar, 4–9 sccm O_2) was analysed by X-ray diffraction. The cubic phase of the YSZ system was identified for all samples (see Table 1). The XRD pattern registered for the sample deposited at 4.0 sccm O_2 flow is presented in Fig. 7. The insert details the area around the angle $2\theta = 25°$. The additional peak of the tetragonal phase ($2\theta = 24.876°$) cannot be observed.

Plasma spraying

The first experiments concerned the precursor powders, whose morphologies are presented in Fig. 8. For the LSM cathode the stoichiometric mixture of precursor oxides, La_2O_3, MnO_2 and $SrCO_3$, was attempted, but the results were not satisfactory even after different combinations of calcinations time and temperatures, and intermediate grindings. The broad size distribution of the powders prevented a uniform flow during the spaying

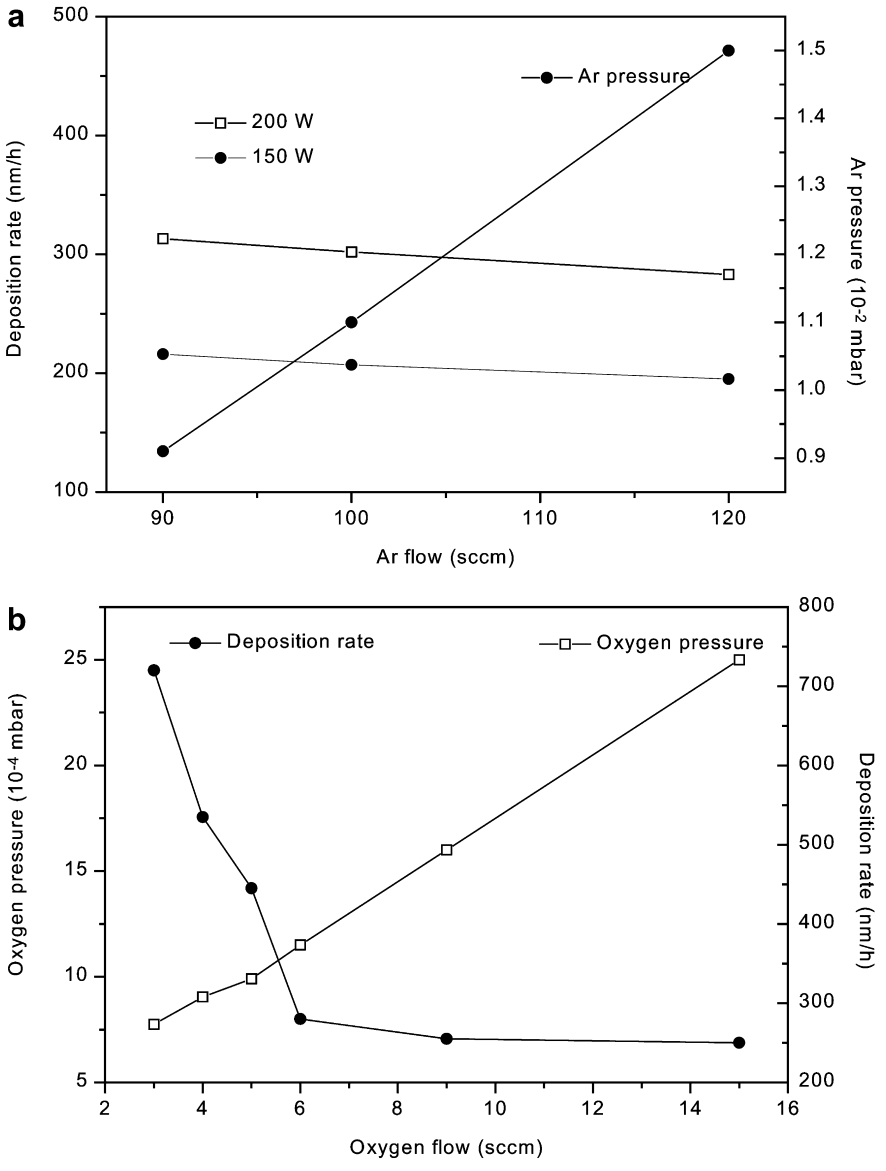

Fig. 2 Deposition rate versus (**a**) argon flow and (**b**) oxygen flow

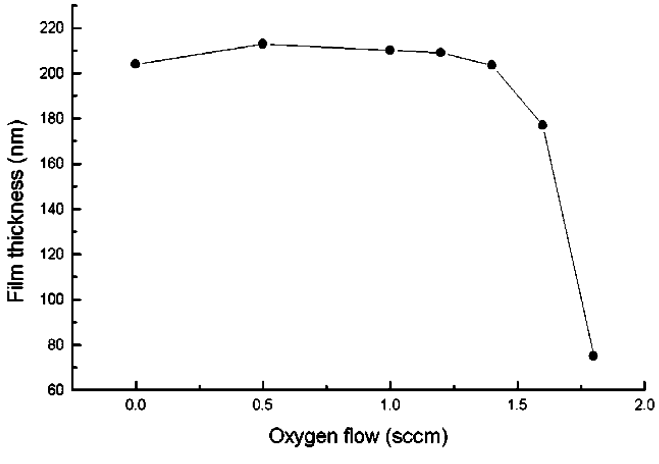

Fig. 3 Influence of the oxygen flow on the film thickness

process, which altered the composition and properties of the sprayed material. Thus, for the next experiments we used the commercially available powders.

Plasma spraying was selected owing to the advantage of depositing the complete electrodes-electrolyte assembly in one integrated process. One of our attempts is shown in Fig. 9, a cross section of a cathode-electrolyte element consisting of a Ni-base alloy plate over which consecutive layers of YSZ (~150 μm thickness) and LSM (~ 350 μm thickness) have been sprayed. In order to be used for SOFC applications, such an assembly needs a porous anode material. To accomplish this we deposited thick films of a powder mixture of YSZ with 2–40 wt% Ni. As the anode material should have low resistivity, the amount of expensive Ni in the mixture must be high. The results obtained for our samples are presented in Table 2. On the other hand, the homogeneity and porosity of the sprayed material were less favourable for higher amounts of Ni. Taking into

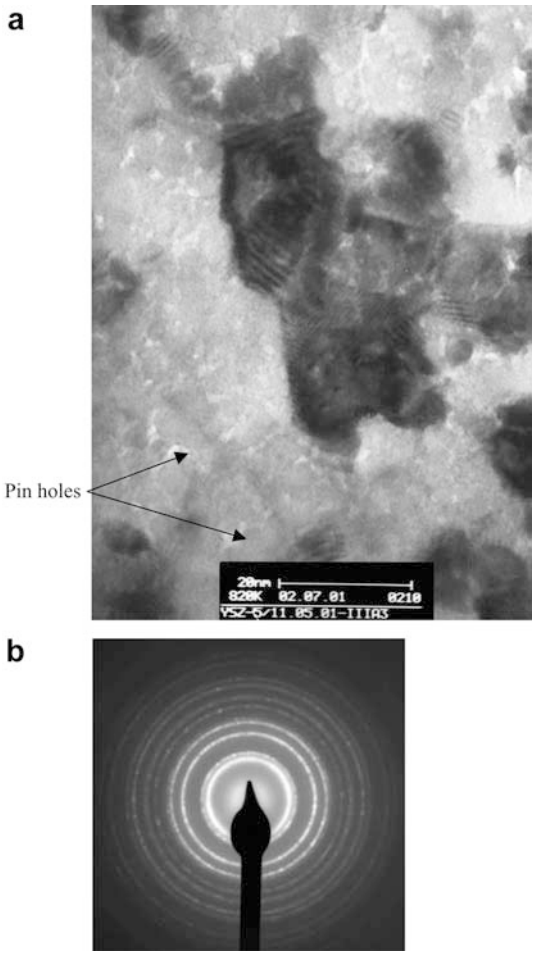

Fig. 4 TEM image of YSZ thin film: (**a**) bright-field image, pinholes between grains of approximately 10 nm diameter; (**b**) electron diffraction image

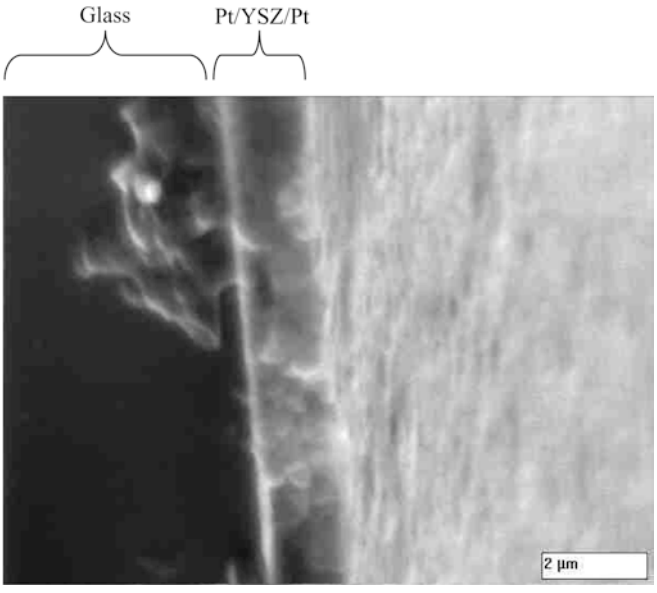

Fig. 5 SEM image of the Pt/YSZ/Pt assembly deposited on glass: Cross section

account all these considerations, work is in progress to find the optimum composition and microstructure of the anode material.

For the cathode-electrolyte assembly in Fig. 9 we have measured the oxygen ion conductivity at 450 °C in the d.c. regime, like in a planar-type limiting current amperometric sensor [8, 9, 10]. In this experiment the $La_{0.8}Sr_{0.2}MnO_3$ is the cathode, the YSZ is the ion-conducting electrolyte and the Ni alloy is the anode. A flow of different concentrations of oxygen in nitrogen carrier gas, adjusted by a MKS Multigas controller 647B, passed the sample and the change of current in dependence on the voltage was measured. The measured signal for different polarizations increased with the oxygen content, stronger in the low concentrations and to a limit for higher amounts of analysed gas (Fig. 10).

The electrical resistivity of the plasma-sprayed YSZ material, deposited on Ni-base alloy plate and coated with a thin film Pt electrode, was analysed by impedance spectroscopy. Some of the results are presented in Fig. 11. Figure 11a shows the impedance spectra at different temperatures, Fig. 11b the measurements at a fixed temperature under various oxygen partial pressures (given in ppm referred to the O_2/N_2 ratio of the gas). The impedance spectra show at any temperature a semicircle at high frequencies and a so-called Warburg spike at low frequencies. The semicircle is asymmetric and represents the ionic conductivity of the material resulting from bulk and grain boundary conductivity [1, 11, 12]. However, this contribution to the sample conductivity is a function of temperature (Fig. 12) and at constant temperature is independent of the oxygen partial pressure (Fig. 11b), as to be expected for an ionic conductor. The low-frequency spikes indicate the charge transfer at the electrode/ceramic interface and can be caused by any diffusion-limited process (such as surface diffusion, humidity effects, diffusion of adsorbed oxygen). A reproducible dependence of this spike on oxygen partial pressure was found starting with 400 °C. The dependence of the charge transfer at active electrodes on oxygen partial pressure is typical for oxygen ion conductors. With increasing oxygen partial pressure the transfer resistance for oxygen decreases (see Fig. 11b). From this we conclude the evidence for oxygen ion conductivity in the plasma-sprayed assembly investigated. From the impedance spectroscopy measurements of the samples described in Table 3 we have calculated the specific resistivity (σ) of the YSZ electrolyte in the temperature range 300–675 °C. According to the Arrhenius equation $\sigma = A\exp(-E_A/kT)$ (where E_A = activation energy, k = Boltzmann constant, T = temperature, and A = constant), the activation energy can be calculated as the slope of the plot $\ln\sigma$ vs. $1/T$, depicted

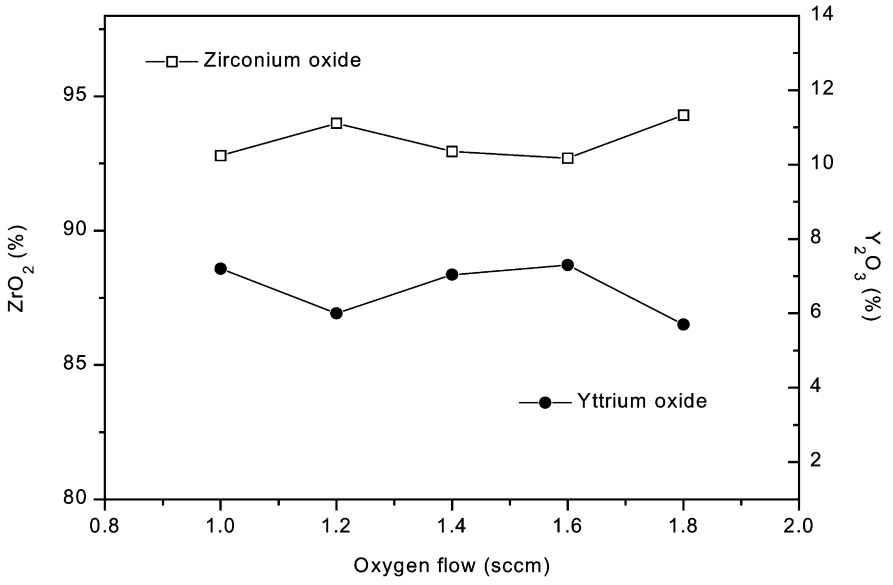

Fig. 6 Chemical composition of YSZ thin film versus oxygen flow

Table 1 2θ diffraction angles ($\lambda = 1.12$ Å) for cubic and tetragonal phases of zirconia, compared with the XRD measurements

Cubic YSZ (JCPDS 30-1468)	Tetragonal ZrO_2 (JCPDS 17-923)	Sample 63 (4 sccm O_2)	Sample 65 (9 sccm O_2)	Sample 66 (6.5 sccm O_2)
21.751	21.811	21.675	21.5	21.55
–	24.876	–	–	–
25.161	25.474	25.375	25.38	25.375
35.881	35.638	35.625	35.68	35.7
42.359	42.445	42.3	42.22	42.475
44.340	44.059	44.15	43.56	43.525
51.672	51.845	51.775	–	51.65528
56.716	56.145	56.625	56.54	56.625

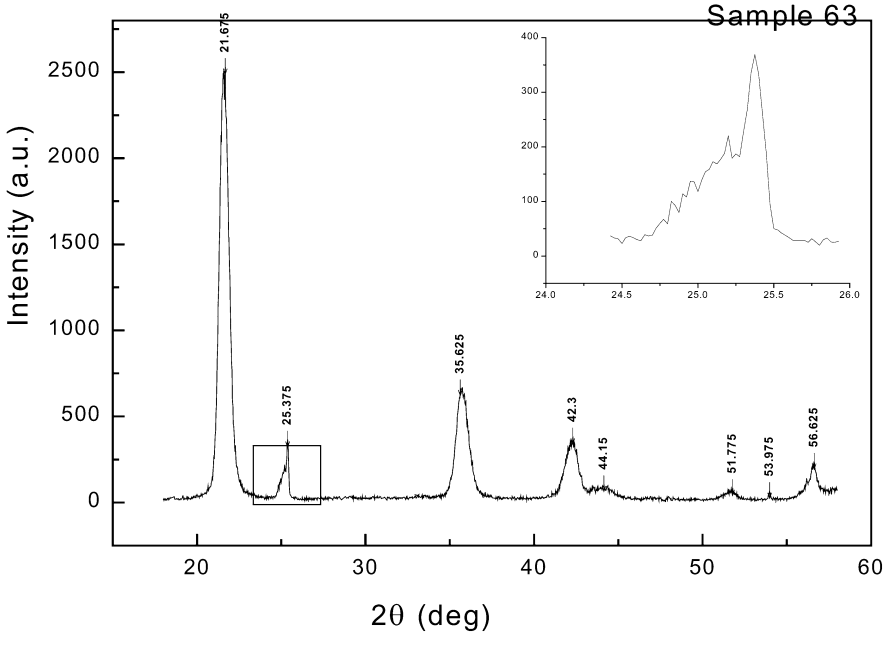

Fig. 7 XRD pattern of the sample 63

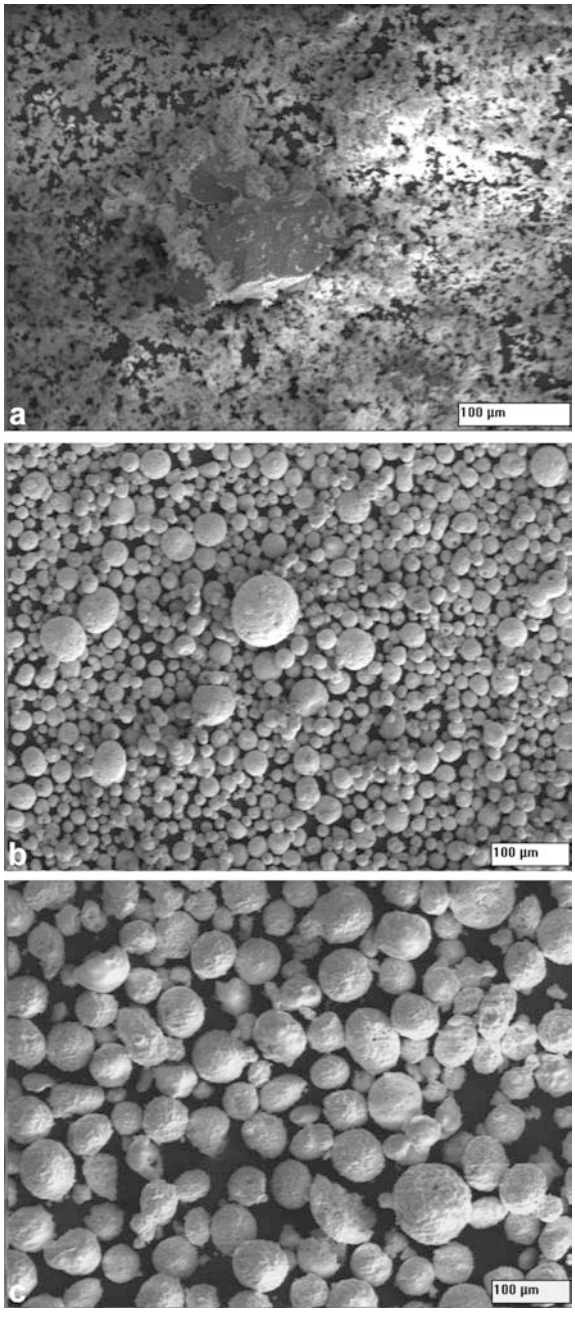

Fig. 8 Morphology of the precursor powders: (**a**) calcined LSM, (**b**) commercially available LSM, (**c**) commercially available YSZ

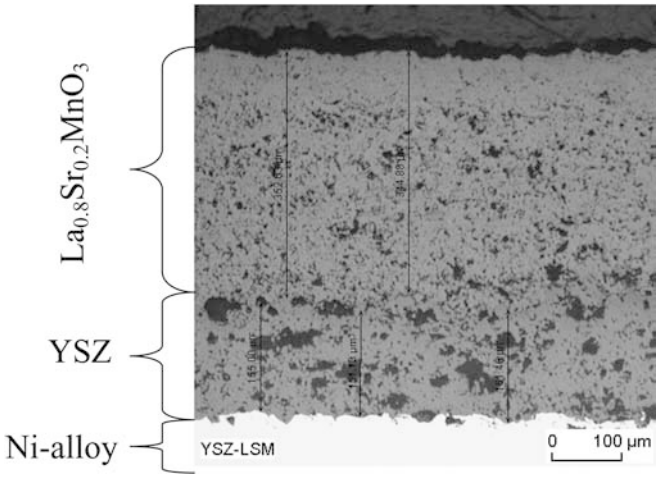

Fig. 9 Cross section of the plasma-sprayed SOFC element

Table 2 Electrical measurements: resistance

Anode material	R (Ω)
YSZ + 5% Ni	1.50–3.50
YSZ + 7.5% Ni	1.70–2.00
YSZ + 10% Ni	0.50–0.90
YSZ + 25% Ni	0.12–0.13
YSZ + 40% Ni	0.10

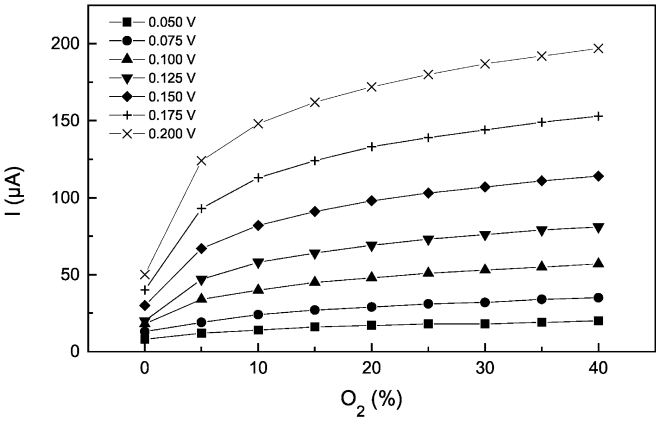

Fig. 10 Oxygen ion conductivity measurements at 450 °C

in Fig. 12. The values are given in Table 3 and are comparable with the reported data [1, 12, 13, 14].

Conclusions

Thin films of YSZ have been deposited by sputtering (r.f. and d.c.) and by plasma spraying, and have been analysed for applications as a solid electrolyte in oxygen gas sensors and SOFCs. Different substrates have been considered in order to provide good adhesion, dense electrolyte films, and mechanical and thermal stability. By optimization of the sputtering parameters a Pt/YSZ/Pt assembly of 1.5 µm thickness and with an electrical resistance of 500 MΩ at room temperature has been obtained.

Plasma spraying was used to deposit the complete electrodes-electrolyte assembly in one integrated process. Spraying of the LSM cathode material from the precursor powders La_2O_3, MnO_2 and $SrCO_3$ was not successful owing to great differences in the grain

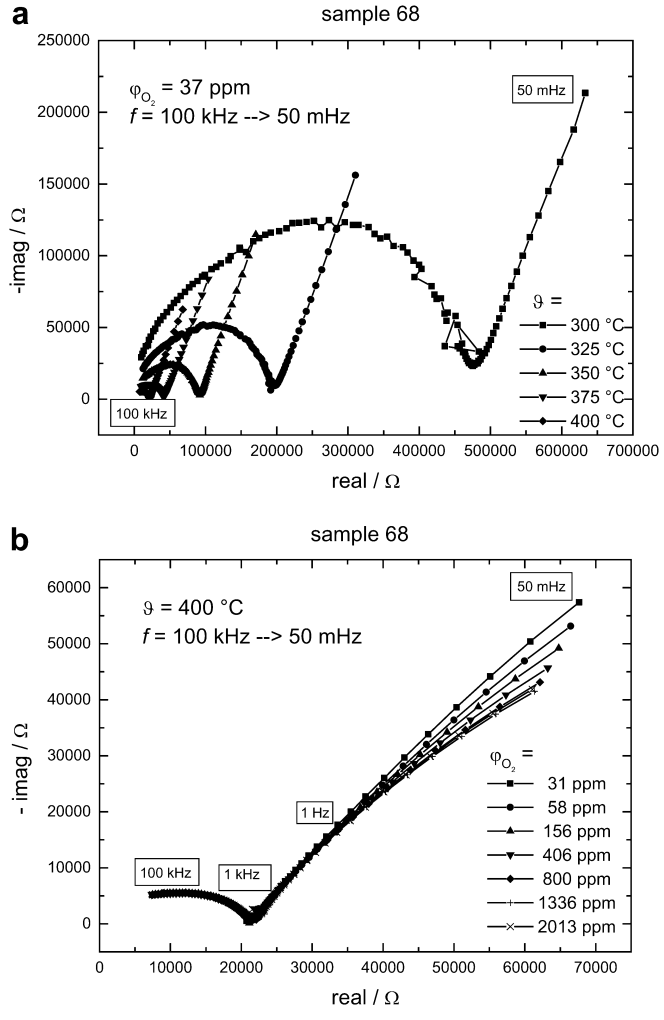

Fig. 11 Impedance diagrams of plasma-sprayed YSZ: (**a**) constant oxygen pressure and different temperatures (300–400 °C); (**b**) at 400 °C and different oxygen pressures

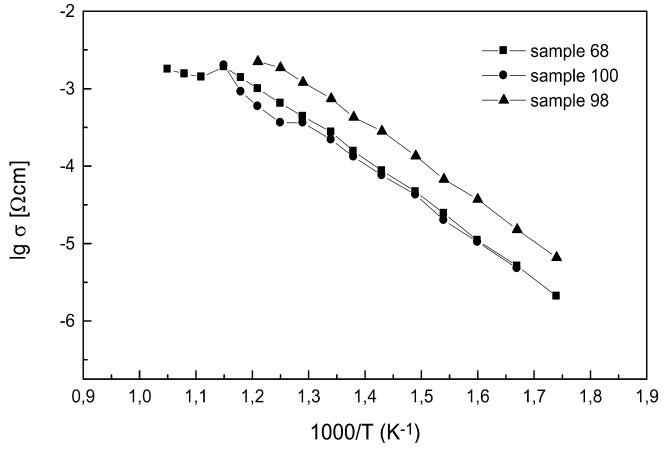

Fig. 12 Activation energy of oxygen ion conductivity

Table 3 Activation energy of oxygen ion conductivity

Sample	Thickness (μm)	E_A (kJ/mol)	E_A (eV)
68	1000	96.3	1.13
100	500	95.0	1.09
98	300	95.3	1.10

dimensions. Better results have been obtained using commercially available powders (LSM of 20–90 μm and YSZ of 50 μm). The sprayed YSZ films have shown oxygen ion conductivity with a reproducible sensitivity on oxygen partial pressure starting at 400 °C and an activation energy of ~1 eV.

Acknowledgements The authors would like to thank Dr Jianu and Dr Nicula for the synchrotron experiments, and Dr Käding for the impedance spectroscopy measurements.

References

1. Aoki M, Chiang Y-M, Kosachki I, Lee LJ-R, Tuller, Liu Y (1996) J Am Ceram Soc 79:1169
2. Badwal SPS, Ciacchi FT, Rajendran S, Drennan J (1998) Solid State Ionics 109:167
3. Bae JW, Park JY, Hwang SW, Yeom GY, Kim KD, Cho YA, Jeon JS, Choi D (2000) J Electrochem Soc 147:2380
4. Chiodelli G, Flor G, Scagliotti M (1996) Solid State Ionics 91:109
5. Florio DZ, Muccillo R (1999) Solid State Ionics 123:301
6. Fonseca FC, Muccillo R (2000) Solid State Ionics 131:301
7. Nakao M, Sato H, Kamimura K, Onuma Y (1996) Proceedings of the international electronic manufacturing technology symposium, New York. IEEE, Piscataway, NJ, pp 162–165
8. Garzon F, Raistrick I, Brosha E, Houlton R, Chung BW (1998) Sens Actuators B 50:125
9. Ishibashi K, Kashima T, Asada A (1993) Sens Actuators B 13–14:41
10. Yu S, Wu Q, Tabib-Azar M, Liu C-C (2002) Sens Actuators B 85:212
11. MacDonald JR (1987) Impedance spectroscopy. Wiley-Interscience, New York
12. Maslov AV, Mezheritsky GS, Moskalev JI, Prilezhaeva IN, Rezvykh IA, Khramushin NI (1997) In: Savadogo O, Roberge PR (eds) Proceedings of the 2nd international symposium on new materials for fuel-cell and modern battery systems, Montreal, Canada. L'Ecole Polytechnique de Montréal, Montréal, pp 125–135
13. Barthel K, Rambert S (1998) Proceedings of the 3rd European solid oxide fuel cell forum, Nantes, France. European Fuel Cell Forum, Oberrohrdorf, pp 11–18
14. Hartmanova M, Thurzo I, Jergel M, Bartos J, Kadlec F, Zelezny V, Tunega D, Kundracik F, Chromik S, Brunel M (1998) J Mater Sci 33:969